ORIGINAL ARTICLE

Active vibration damping for manufacturing machines using additional cable mechanisms: conceptual design

Zdeněk Neusser[1] · Martin Nečas[1] · Jan Pelikán[1] · Vít Pawlik[1] · Petr Beneš[1] · Jan Zavřel[1] · Jiří Volech[1] · Vojtěch Halamka[1] · Martin Machálka[2] · Michael Valášek[1] · Zbyněk Šika[1]

Abstract

Undesired vibration is a common issue when dealing with manufacturing machines, especially when dealing with thin structures. To decrease the external disturbance sensitivity of such systems, represented for example by machine tool quill, the auxiliary cable structure is attached to the system. The auxiliary cable structure increases system damping and decreases undesired structure vibrations by the passive or active way, depending on the deployment and purpose. In this article, cables are attached to the end-effector to suppress undesired vibrations and related experimental stand is prepared. Experimental stand parameters are identified using least square method. The control strategy using pole placement is presented and its suitability is verified using external disturbance force. The frequency analysis shows the promising behaviour of controlled cable structure attached to the original system as well as the experimental results.

Keywords Flexible structure · Vibration suppression · Machine tool · Cable structure

1 Introduction

The motivation for solving the problem of thin, flexible structure vibration is related to the industrial needs. The achievable positioning accuracy of the end point under dynamic load is crucial for these structures. A typical example of such structure is machine tool quill; it has a thin shape with limited stiffness. This problem can be solved using the auxiliary cable structures, which are not difficult to attach to the specific point of the flexible structure. The desired motion of whole system can be achieved by appropriate control actions at the cable structure.

For undesired vibration suppression, dampers are often used, either a passive damper tuned to a specific frequency [1, 2] or an active damper which is able to influence a wide band of frequencies. Publication [3] describes various options for dealing with vibration, such as semi-active vibration insulation or active vibration damper for machine tools. Work [4] deals with the design of a 3-degrees-of-freedom active vibration absorber for a robot arm. A special case of an active damper with delayed feedback, called delayed resonator, which is able to perfectly suppress vibration of the primary structure, has been studied extensively [5, 6], also with acceleration feedback [7] or combination of position, velocity, and acceleration feedback [8]. Suppression of multiple frequencies is investigated in [9] and [10]. In [11, 12], the concept has been extended for planar vibration suppression. The under-actuated mechanical systems' residual vibration cancelation is investigated in [13, 14]. The papers show the wide range of vibration suppression methods, which often need significant mechanical modification of the machine working point (TCP).

In manufacturing machines, the vibrations can be dealt with by modifying the work-piece holder [15], the tool holder [16, 17], or the tool itself [18]. In [19], a composite boring bar is developed to dampen vibrations of the tool and in [20] a variable stiffness vibration absorber is put inside the tool. The vibration can also be reduced by modifying the fixture, for example partly submerging the work-piece in magnetorheological fluid [21]. In [22], vibration of the work-piece holder is dampened using a magnetorheological damper. However, using existing actuators with a new control strategy allows to suppress vibrations without adding

✉ Zdeněk Neusser
zdenek.neusser@fs.cvut.cz

1 Department of Mechanics, Biomechanics and Mechatronics, Faculty of Mechanical Engineering, Czech Technical University in Prague, Technická 4, Prague 160 00, Czech Republic

2 TAJMAC-ZPS, a. s., třída 3. května 1180, Zlín 763 02, Czech Republic

additional mass to any part of the machine [23]. Another solution is proposed in [24] combining input shaping with the addition of servo control for uncertainties and disturbances removing. In [25], the prediction of the position error is used to modify the input command of a dual-driving gantry-type machine to improve accuracy. In [26], a control strategy is designed to reduce vibrations of the tip of a long and flexible manipulator. These papers propose direct placement of additional actuators, change of materials, or complicated control strategies. Altogether these ways need fundamental changes of the machine structure or machine control concept.

Actuators in the form of piezoelectric patches have been used to reduce the vibration of flexible beams in [27] and [28] using a delay-feedback controller, and in [29] using a self-organizing map-based controller. Work [30] studies the dynamics of a cantilever stayed beam. The dynamic properties of a cable-beam system with cantilever beam and the wires connected to its tip have been explored with wires being perpendicular in [31] and parallel [32]. A flexible manipulator with two cables is studied in [33]. Publication [34] deals with vibration of a tapered cantilever beam with a wire connected to its tip. The wires, in combination with a control strategy, can be used to suppress vibrations of the beam, such as in [35]. To be able to transfer force through a cable, the dynamical properties of the cable must be also known and included in the control. The behaviour of a fibre has been modelled with respect to fibre mass, stiffness, and damping [36–39]. In [40], stiffness of cables with large strains has been studied. These papers deal with the cable properties, appropriate models, or control without machine tool context.

An approach to studying the position accuracy and vibrations of a high-frequency moving robot arm has been proposed in [41]. In [42], vibrations of cable mechanisms and their properties in general have been studied and an optimal Fuzzy-PID control developed, focusing on optimizing settling time, maximum control force, and energy consumption. In [43], an adaptive robust control is developed for cable-driven parallel robots for trajectory tracking. The machine redundancy is investigated in [44] and control with sliding mode control is presented in [45]. Control of mechanical systems with particular cable application is shown in the papers.

The presented paper brings a new idea of the vibration suppression of production machine working point (TCP). Several types of machine tools with a large workspace suffer from unwanted vibrations of long and heavy movable parts. These vibrations are very often composed mainly from bending vibration with first eigenfrequency of such parts and their additional suppression can improve material removal abilities and spindle power utilization in the whole working span. The novelty of concept is based on adding cables controlled by standard rotational drives, which create the auxiliary parallel structure and bring additional damping force near to the machine working point (TCP). According to the best knowledge of the authors, the investigation of the machine tools cable-based vibration suppression is so far very limited. Moreover, the cables can be easily reconfigured and the original workspace of machine is almost preserved. The simplified model of machine tool structure is used, the model is prepared, and the control law is established. The simulation experiment with state feedback is performed as well as experimental work.

This concept can help many types of machines with an upper gantry and a slim headstock box-in-box positioned structure, e.g. machines from the TAJMAC-ZPS portfolio. This approach leads to increased material removal capabilities and the use of spindle power over the entire working range, or allows the design of the machine tool to be lightened.

The paper is organized as follows. In the first section, the motivation and literature survey is prepared, the second section shows the experimental setup model with identification of all important parts, and the system is linearized. The third section is dedicated to the vibration damping analysis with two ways of drive control and also shows the simulation experiment of the resulting structure. The fourth section is dedicated to experimental results. The last section concludes the work.
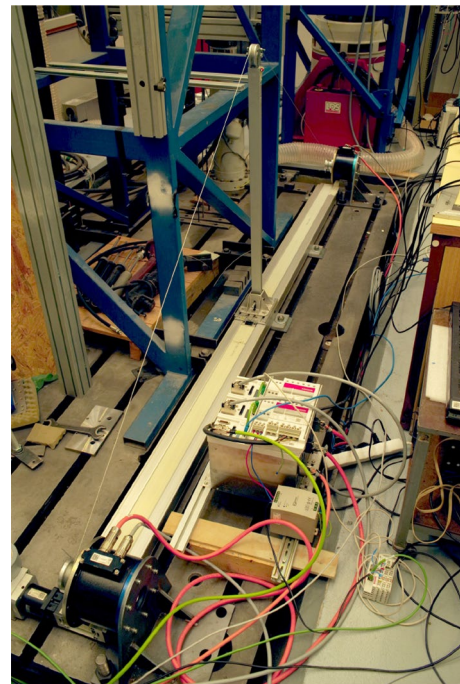

Fig. 1 Experimental stand

2 Experimental setup modelling

A physical model of experimental setup is derived in this section. To explore the concept of suppressing vibrations using additional cables, simple experimental demonstrator was prepared as shown in Fig. 1. The demonstrator is created in order to include the main dynamic properties of the abovementioned machine tools with a large workspace and long heavy movable parts.

Based on the stand, a simplified simulation model was created; Fig. 2 shows model parameters and coordinates. The torques M_i are exerted by electric servo drives with inputs u_i. The cart movement is prescribed as separate input, and the cable mass is neglected. A free body diagram method is chosen to assemble the equations of motion. Forces and torques acting on each body of the system and coordinates describing their movement are depicted in Fig. 3. Equations of motion resulting from Fig. 3 are

$$
\begin{aligned}
I_1\ddot{\varphi}_1 &= M_1 - F_1 r_1 - b_{M1}\dot{\varphi}_1 \\
I_2\ddot{\varphi}_2 &= M_2 + F_2 r_2 - b_{M2}\dot{\varphi}_2 \\
m\ddot{x}_n &= -F + F_2\cos\alpha_2 - F_1\cos\alpha_1
\end{aligned}
\tag{1}
$$

where coordinates φ_1 and φ_2 are electric servo drive rotor angular positions, coordinate x_n is horizontal coordinate of the TCP, and x coordinate represents horizontal position of the cart.

Equations of motion (1) contain inertial forces, cable forces, elastic beam force, damping forces with damping coefficients b_{M1} and b_{M2}, and cable angles α_i. Forces F, F_1 and F_2 can be expressed as

$$
\begin{aligned}
F_1 &= \frac{k_1}{L_1}\xi_1 + \frac{b_1}{L_1}\dot{\xi}_1 \\
F_2 &= \frac{k_2}{L_2}\xi_2 + \frac{b_2}{L_2}\dot{\xi}_2 \\
F &= k(x_n - x) + b(\dot{x}_n - \dot{x})
\end{aligned}
\tag{2}
$$

Determination of cable extensions ξ_i in Eq. (2) is based on Fig. 4. The left part of the picture depicts the derivation of angle α_1 measured from the x axis, and the right part shows length of cable including segments wound on pulleys. Stiffness of both cables is presumed to be the same and equals to k_L, $k_1 = k_2 = k_L$. Stiffness is in reciprocal proportion to the cable length as well as the cable dampings b_1 and b_2, $b_1 = b_2 = b_L$.

Extension of cables (longitudinal deformation) equals to difference of actual cable length (including small cable segments on the pulleys, see Fig. 4 right) and initial length of the cable:

$$
\begin{aligned}
\xi_1 &= L_1 - L_{10} + (r - r_1)(\alpha_1 - \alpha_{10}) + \varphi_1 r_1 \\
\xi_2 &= L_2 - L_{20} + (r - r_2)(\alpha_2 - \alpha_{20}) - \varphi_2 r_2
\end{aligned}
\tag{3}
$$

Symbols L_{10}, L_{20} and α_{10}, α_{20} in Eq. (3) correspond to initial cable lengths and cable angles, respectively. Actual lengths and angles of the cables can be derived from Fig. 4 as
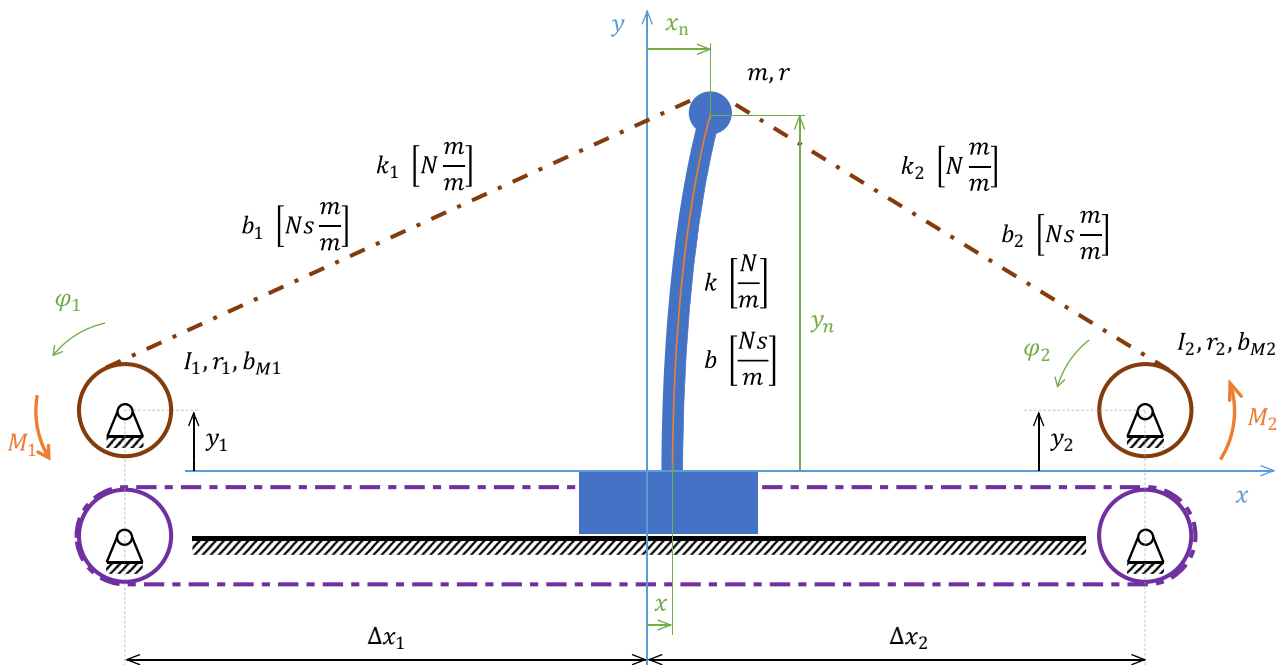

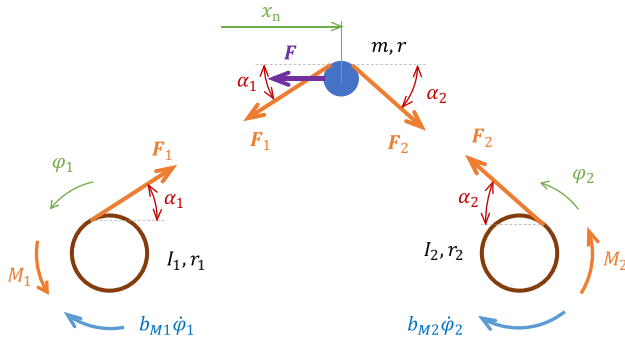**Fig. 2** Mechanical model of the experimental stand

Fig. 3 Free body diagram

$$L_1 = \sqrt{(x_n + \Delta x_1)^2 + (y_n - y_1)^2 - (r_1 - r)^2}$$

$$L_2 = \sqrt{(\Delta x_2 - x_n)^2 + (y_n - y_2)^2 - (r_2 - r)^2}$$

$$\alpha_1 = \beta + \gamma = \arctan\left(\frac{y_n - y_1}{x_n + \Delta x_1}\right) + \arctan\left(\frac{r_1 - r}{L_1}\right) \quad (4)$$

$$\alpha_2 = \arctan\left(\frac{y_n - y_2}{\Delta x_2 - x_n}\right) + \arctan\left(\frac{r_2 - r}{L_2}\right)$$

with the only time-dependent variable x_n, the rest of the parameters are constants of the structure design. Radii r_1 and r_2 are first and second motor cable pulleys, and r is the radius of beam tip cable pulley, where the cables are fixed. The beam deformation is assumed to be small; therefore, the beam tip coordinate y_n does not change its value.

Cable extension velocities $\dot{\xi}_1$ and $\dot{\xi}_2$ used in Eq. (2) are time derivative of Eq. (3) and particular members of Eq. (4):

$$\dot{\xi}_1 = \dot{L}_1 + (r - r_1)\dot{\alpha}_1 + \dot{\varphi}_1 r_1$$
$$\dot{\xi}_2 = \dot{L}_2 + (r - r_2)\dot{\alpha}_2 - \dot{\varphi}_2 r_2 \quad (5)$$

The electromagnetic field in the BLDC drives produce the rotor torques M_1 and M_2. The torque is modelled as proportional to the stator armature current:

$$M_1 = k_{t1} i_1$$
$$M_2 = k_{t2} i_2 \quad (6)$$

with the current constants k_{t1} and k_{t2} of the first and second motor.

The moments of inertia I_1 and I_2, the equivalent beam mass m, damping coefficients b_{M1} and b_{M2} from the equations of motion in Eq. (1), stiffnesses k and k_L, damping coefficients b and b_L from the forces in Eq. (2), and parameters k_{t1} and k_{t2} from (6) are subject of identification process while being unknown.

2.1 System parameters identification

Model parameters are assessed in this sub-section. The important property of all parameters lies in the linearity. They create a system of linear equations (mostly time dependent). Due to the measurement of other system parameters than just inputs and output, the identification process is separated into three parts: beam identification, cable properties identification, and drive 1, drive 2 identification.

The beam properties are obtained from the measurement of initially deflected beam. An accelerometer is placed at the end point of the beam and free oscillations are performed due to the initial beam deflection. The measurement is performed by an accelerometer and oscilloscope. For the cable
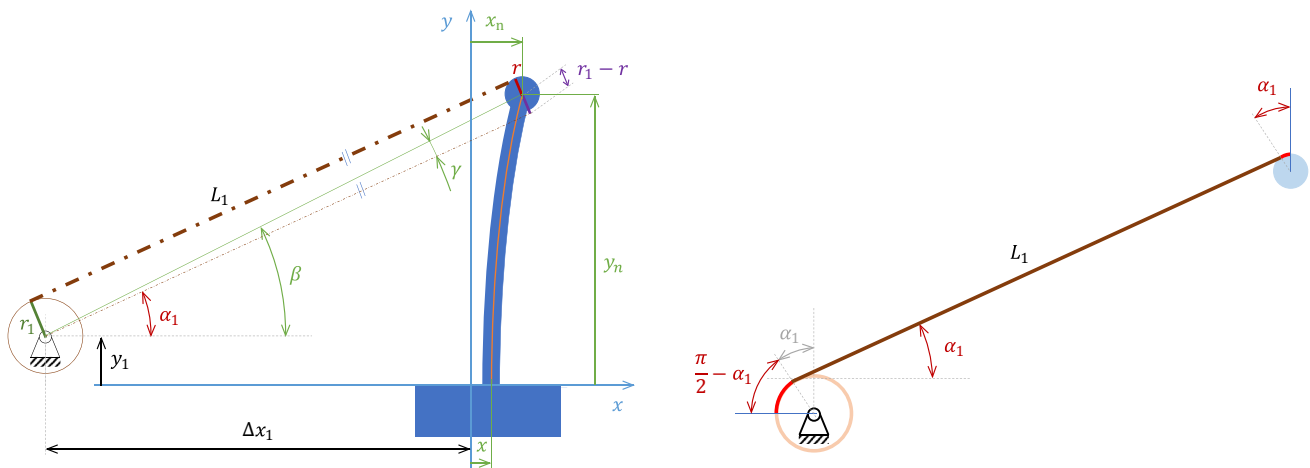

Fig. 4 Derivation of cable angle (left) and cable length (right)

and electric drives with drive controller part identification is performed following experiment. The sweep cosine signal is an input at first drive and constant pre-load is applied at the second drive. The similar experiment is performed with constant pre-load at first drive and sweep cosine signal at the second drive. The excitation frequency range is from the 0.5 up to 30Hz, which is a reasonable range for expected machine tool movement excitation. The horizontal position of the beam end-point and cart position is measured by laser-tracker, and the drive angular positions are measured by drive internal measurement sensors.

2.1.1 Beam properties

The beam fixed to the cart is modelled as a cantilever and it dominantly vibrates at its first eigenmode. The identification of k, b, and m is based on analytical solution of beam deflection and experimental data.

The experiment on Fig. 5 shows unforced beam oscillations measured by an accelerometer. On the left part of the figure, two beam oscillation periods are measured and damped system eigenfrequency is obtained in Eq. (7).

$$\Delta t = 0.185 \ s$$
$$f_{beam_d} = \frac{2}{\Delta t} = 10.8108 \ Hz \tag{7}$$

Damping ratio is obtained from Fig. 5 right part. The mean accelerometer output signal value is $Signal_{mean} = 4.42mV$, the peak value at the oscillation beginning is $Signal_1 = 608mV$, and the oscillation amplitude after $\Delta t_{sig} = 6.28s$ is $Signal_2 = 88mV$. Logarithmic decrement δ is natural logarithm of magnitudes ratio:

$$\delta = \ln \frac{Signal_1 - Signal_{mean}}{Signal_2 - Signal_{mean}} = 1.977 \tag{8}$$
$$\delta = 2\pi f_{beam_d} \Delta t_{sig} \kappa$$

with κ used in the damping ratio ζ evaluation:

$$\kappa = \frac{\delta}{2\pi f_{beam_d} \Delta t_{sig}}$$
$$\zeta = \frac{\kappa}{\sqrt{\kappa^2 + 1}} = 4.635 \cdot 10^{-3} \tag{9}$$

Using damped system eigenfrequency in Eq. (7) and damping ratio in Eq. (9), the undamped beam eigenfrequency (further just eigenfrequency) is obtained:

$$f_{beam} = \frac{f_{beam_d}}{\sqrt{1 - \zeta^2}} = 10.8109 \ Hz \tag{10}$$

Damping ratio and eigenfrequency are not sufficient to obtain k, b, and m parameters of the reduced beam model. The equation of fixed beam horizontal deflection allows us to calculate beam horizontal stiffness at beam reduced mass position. Beam length $L = 0.95m$, material young modulus $E = 70 \cdot 10^9 Pa$, and cross-section quadratic moment $J = 1.88 \cdot 10^{-8} m^4$ are required inputs for beam stiffness calculation:

$$k = \frac{3EJ}{L^3} = 4604.75 \frac{N}{m} \tag{11}$$

Then using homogeneous part comparison of the third equation of motion from Eq. (1) with substituted force F from Eq. (2)

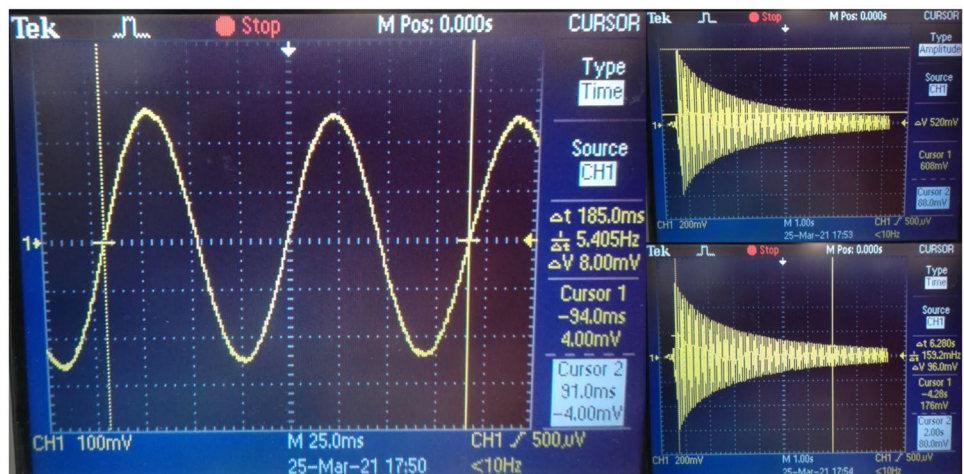$$\ddot{x}_n + \frac{b}{m}\dot{x}_n + \frac{k}{m}x_n = Rhs$$
$$\ddot{x}_n + 2\zeta(2\pi f_{beam})\dot{x}_n + (2\pi f_{beam})^2 x_n = Rhs \tag{12}$$

beam equivalent mass m and beam damping b are derived:

$$m = \frac{k}{(2\pi f_{beam})^2} = 0.998 \ kg$$
$$b = 2\zeta(2\pi f_{beam})m = 0.63 \ \frac{Ns}{m} \tag{13}$$

Fig. 5 Identification of beam parameters

2.1.2 Cable properties

The cable used at experimental stand at Fig. 1 is a lightweight wound metallic cable characterized by its stiffness k_L and damping b_L. The cable is the same on both sides of the experimental setup. The cable properties identification is based on the experimental measurement. Sweep cosine function is introduced at drives with prestress preventing the cable unloading. The inputs (angular positions φ_1 and φ_2) and the horizontal position of beam TCP point x_n as well as cart position x are recorded.

The equation of motion, taken into account for the identification analysis, is the third one of the set of Eq. (1). Introducing the forces Eq. (2) into this particular equation, it is obtained:

$$m\ddot{x}_n + b\left(\dot{x}_n - \dot{x}\right) + k\left(x_n - x\right) =$$
$$= k_L\left(\frac{\xi_2}{L_2}\cos\alpha_2 - \frac{\xi_1}{L_1}\cos\alpha_1\right) + b_L\left(\frac{\dot{\xi}_2}{L_2}\cos\alpha_2 - \frac{\dot{\xi}_1}{L_1}\cos\alpha_1\right) \tag{14}$$

where unknown parameters k_L and b_L are in linear combination. Other parameters and terms are known or could be derived from the measured data and its numeric time derivative. Numeric time derivative is amended with non-causal zero-phase low pass data filtering.

Data acquisition and further processing keeps the measurement sampling frequency $f_s = 1kHz$. The Eq. (14) is expanded in time and the following matrices are created:

$$\mathbb{U} = \begin{bmatrix} m\ddot{x}_n(0) + b\left(\dot{x}_n(0) - \dot{x}(0)\right) + k\left(x_n(0) - x(0)\right) \\ m\ddot{x}_n(\Delta t) + b\left(\dot{x}_n(\Delta t) - \dot{x}(\Delta t)\right) + k\left(x_n(\Delta t) - x(\Delta t)\right) \\ \vdots \\ m\ddot{x}_n(n\Delta t) + b\left(\dot{x}_n(n\Delta t) - \dot{x}(n\Delta t)\right) + k\left(x_n(n\Delta t) - x(n\Delta t)\right) \end{bmatrix} \tag{15}$$

$$\mathbb{V}_1 = \begin{bmatrix} \frac{\xi_2(0)}{L_2(0)}\cos\alpha_2(0) - \frac{\xi_1(0)}{L_1(0)}\cos\alpha_1(0) \\ \frac{\xi_2(\Delta t)}{L_2(\Delta t)}\cos\alpha_2(\Delta t) - \frac{\xi_1(\Delta t)}{L_1(\Delta t)}\cos\alpha_1(\Delta t) \\ \vdots \\ \frac{\xi_2(n\Delta t)}{L_2(n\Delta t)}\cos\alpha_2(n\Delta t) - \frac{\xi_1(n\Delta t)}{L_1(n\Delta t)}\cos\alpha_1(n\Delta t) \end{bmatrix}$$

$$\mathbb{V}_2 = \begin{bmatrix} \frac{\dot{\xi}_2(0)}{L_2(0)}\cos\alpha_2(0) - \frac{\dot{\xi}_1(0)}{L_1(0)}\cos\alpha_1(0) \\ \frac{\dot{\xi}_2(\Delta t)}{L_2(\Delta t)}\cos\alpha_2(\Delta t) - \frac{\dot{\xi}_1(\Delta t)}{L_1(\Delta t)}\cos\alpha_1(\Delta t) \\ \vdots \\ \frac{\dot{\xi}_2(n\Delta t)}{L_2(n\Delta t)}\cos\alpha_2(n\Delta t) - \frac{\dot{\xi}_1(n\Delta t)}{L_1(n\Delta t)}\cos\alpha_1(n\Delta t) \end{bmatrix} \tag{16}$$

with $\Delta t = \frac{1}{f_s}$ and $n + 1$ measured points. The overall set created from the measurement data has unknown parameters formed in the vector:

$$\mathbb{U} = \begin{bmatrix} \mathbb{V}_1 & \mathbb{V}_2 \end{bmatrix} \begin{bmatrix} k_L \\ b_L \end{bmatrix} \tag{17}$$

Unknowns k_L and b_L cannot be evaluated directly (number of measurement points is significantly higher than number of unknowns), but they are obtained using least square method leading to pseudo inversion assembly.

$$\begin{bmatrix} k_L \\ b_L \end{bmatrix} = \left(\begin{bmatrix} \mathbb{V}_1 & \mathbb{V}_2 \end{bmatrix}^T \begin{bmatrix} \mathbb{V}_1 & \mathbb{V}_2 \end{bmatrix}\right)^{-1} \begin{bmatrix} \mathbb{V}_1 & \mathbb{V}_2 \end{bmatrix}^T \mathbb{U} \tag{18}$$

Resulting stiffness $k_L = 16432\frac{Nm}{m}$ and damping $b_L = 131\frac{Nms}{m}$ are verified in the simulation experiment, where the Eq. (14) has angles φ_1, φ_2 and cart position x as inputs. Comparisons of simulated beam position with experimental beam position measurement are at Figs. 6 and 7. The figures show the time behaviour of beam TCP position (x_n): the experimental data, simulation data, and their difference as absolute error. Figure 6 presents data based on the engine 1 excitation, and Fig. 7 presents the data from engine 2 excitation. System drift at low frequencies (less than $0.3Hz$) is subtracted.

The comparison of model simulation and experimental behaviour in frequency domain is in Fig. 8. The frequency content is similar, the magnitudes slightly differs.

### 2.1.3 Electric drives properties

The identification of electric drives parameters is based on the similar experiment as in Sect. 2.1.2. Drive mechanical parameters are according to Fig. 2 rotor moments of inertia I_1, I_2, bearing damping b_{M1}, b_{M2} and current constants k_{t1}, k_{t2} from Eq. (6). The inputs (winding currents i_1 and i_2), rotor angular positions φ_1, φ_2 and the horizontal position of beam TCP point x_n are recorded.

The equations of motion, taken into account for the identification analysis, are the first and the second of the set of Eq. (1). Introducing the forces in Eq. (2) and electromagnetic moments in Eq. (6) into those particular equations, it is obtained:

$$\left(\frac{k_L}{L_1}\xi_1 + \frac{b_L}{L_1}\dot{\xi}_1\right)r_1 = k_{t1}i_1 - I_1\ddot{\varphi}_1 - b_{M1}\dot{\varphi}_1$$
$$-\left(\frac{k_L}{L_2}\xi_2 + \frac{b_L}{L_2}\dot{\xi}_2\right)r_2 = k_{t2}i_2 - I_2\ddot{\varphi}_2 - b_{M2}\dot{\varphi}_2 \tag{19}$$

where unknown parameters $k_{t1,2}$, $I_{1,2}$ and $b_{M1,2}$ are in linear combination. Other parameters and terms are known or could be derived from the measured data and its numeric time derivative. Numeric time derivative is amended with non-causal zero-phase low pass data filtering as in the previous case.

Data acquisition and further processing keeps the measurement sampling frequency $f_s = 1kHz$. The Eq. (19) are expanded in the measurement time and following matrices are created:
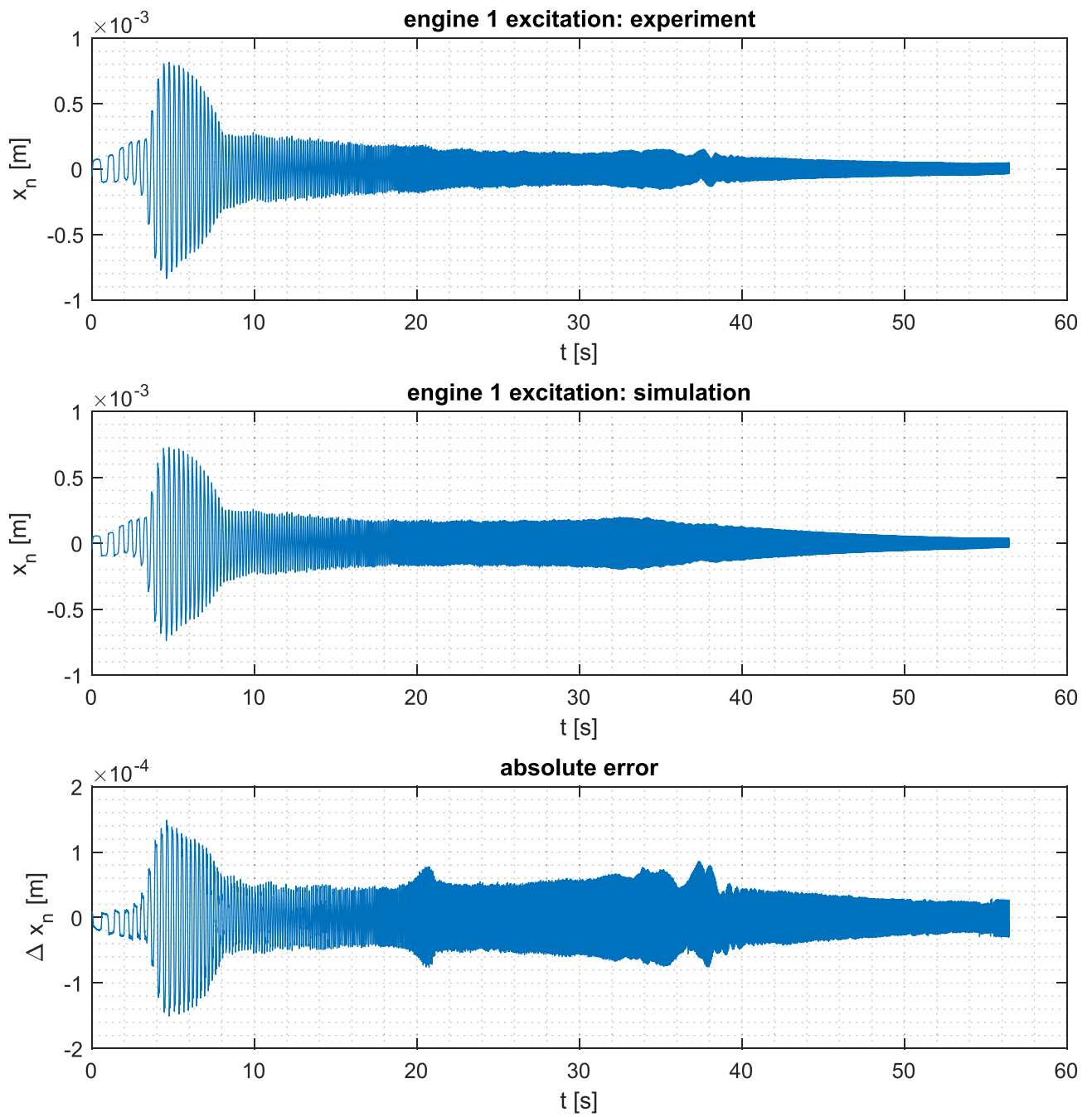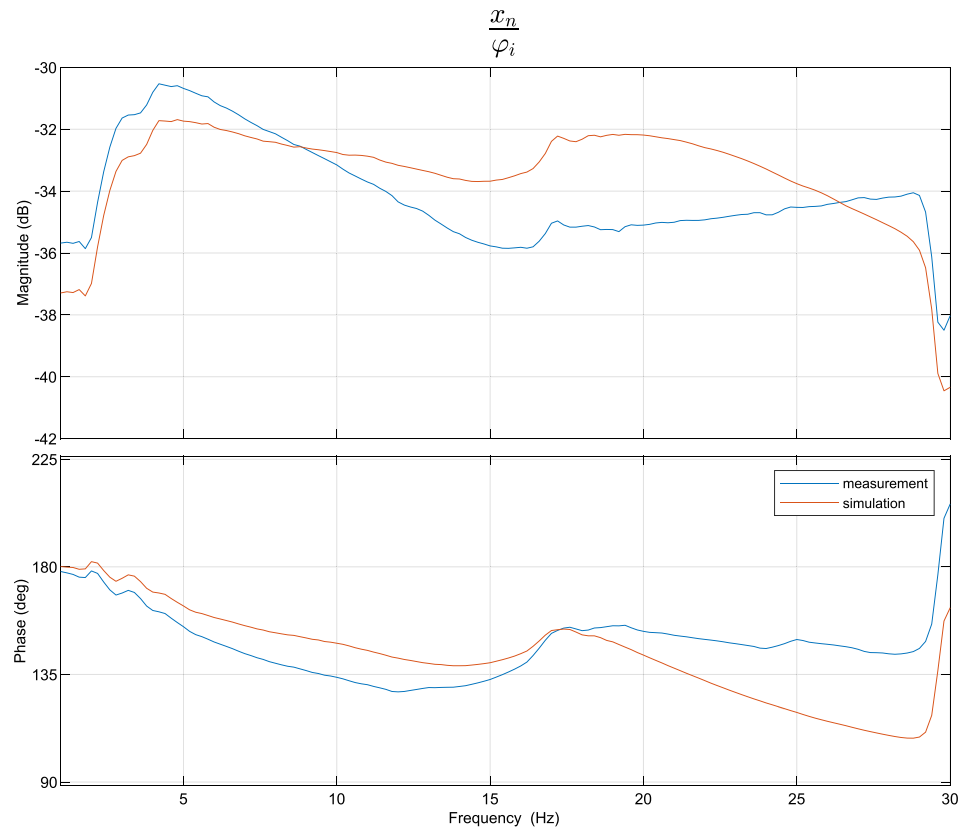
Fig. 6 Verification of identified model: cable parameters, motor 1 excitation
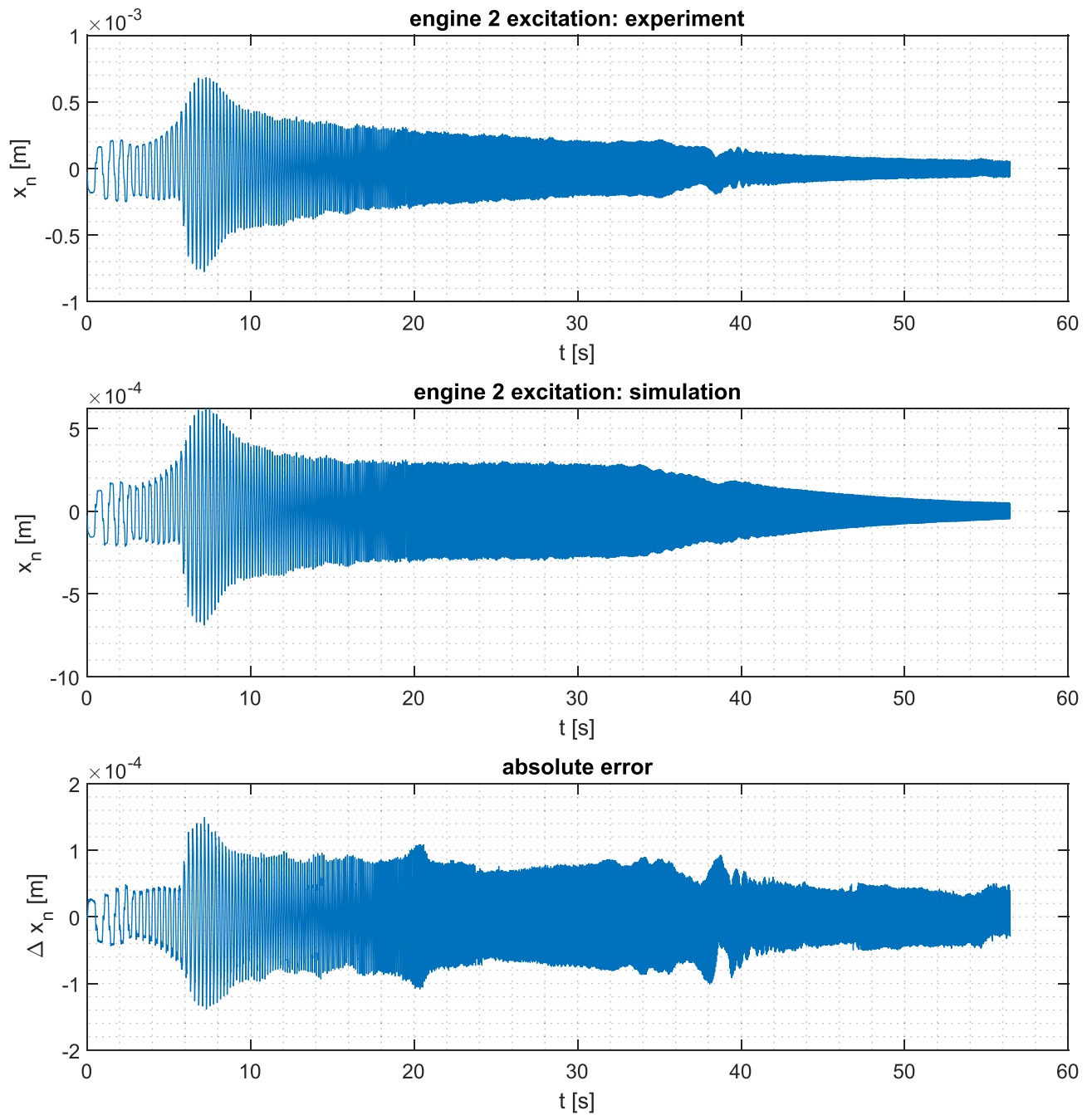
Fig. 7 Verification of identified model: cable parameters, motor 2 excitation

Fig. 8 Verification of identified model: cable parameters, frequency analysis

$$\frac{x_n}{\varphi_i}$$

$$
\mathbb{U} = \begin{bmatrix}
\left(k_L \frac{\xi_1(0)}{L_1(0)} + b_L \frac{\dot\xi_1(0)}{L_1(0)} \right) r_1 \\
\vdots \\
\left(k_L \frac{\xi_1(n\Delta t)}{L_1(n\Delta t)} + b_L \frac{\dot\xi_1(n\Delta t)}{L_1(n\Delta t)} \right) r_1 \\
-\left(k_L \frac{\xi_2(0)}{L_2(0)} + b_L \frac{\dot\xi_2(0)}{L_2(0)} \right) r_2 \\
\vdots \\
-\left(k_L \frac{\xi_2(n\Delta t)}{L_2(n\Delta t)} + b_L \frac{\dot\xi_2(n\Delta t)}{L_2(n\Delta t)} \right) r_2
\end{bmatrix}
\tag{20}
$$

$$
\mathbb{V} = \begin{bmatrix}
i_1(0) & -\ddot\varphi_1(0) & -\dot\varphi_1(0) & 0 & 0 & 0 \\
\vdots & \vdots & \vdots & \vdots & \vdots & \vdots \\
i_1(n\Delta t) & -\ddot\varphi_1(n\Delta t) & -\dot\varphi_1(n\Delta t) & 0 & 0 & 0 \\
0 & 0 & 0 & i_2(0) & -\ddot\varphi_2(0) & -\dot\varphi_2(0) \\
\vdots & \vdots & \vdots & \vdots & \vdots & \vdots \\
0 & 0 & 0 & i_2(n\Delta t) & -\ddot\varphi_2(n\Delta t) & -\dot\varphi_2(n\Delta t)
\end{bmatrix}
\tag{21}
$$

with $\Delta t = \frac{1}{f_s}$ and $n+1$ measured points, as in the previous case. Unknown parameters are placed into the vector:

$$
\mathbb{U} = \mathbb{V} \begin{bmatrix} k_{t1} \\ I_1 \\ b_{M1} \\ k_{t2} \\ I_2 \\ b_{M2} \end{bmatrix}
\tag{22}
$$
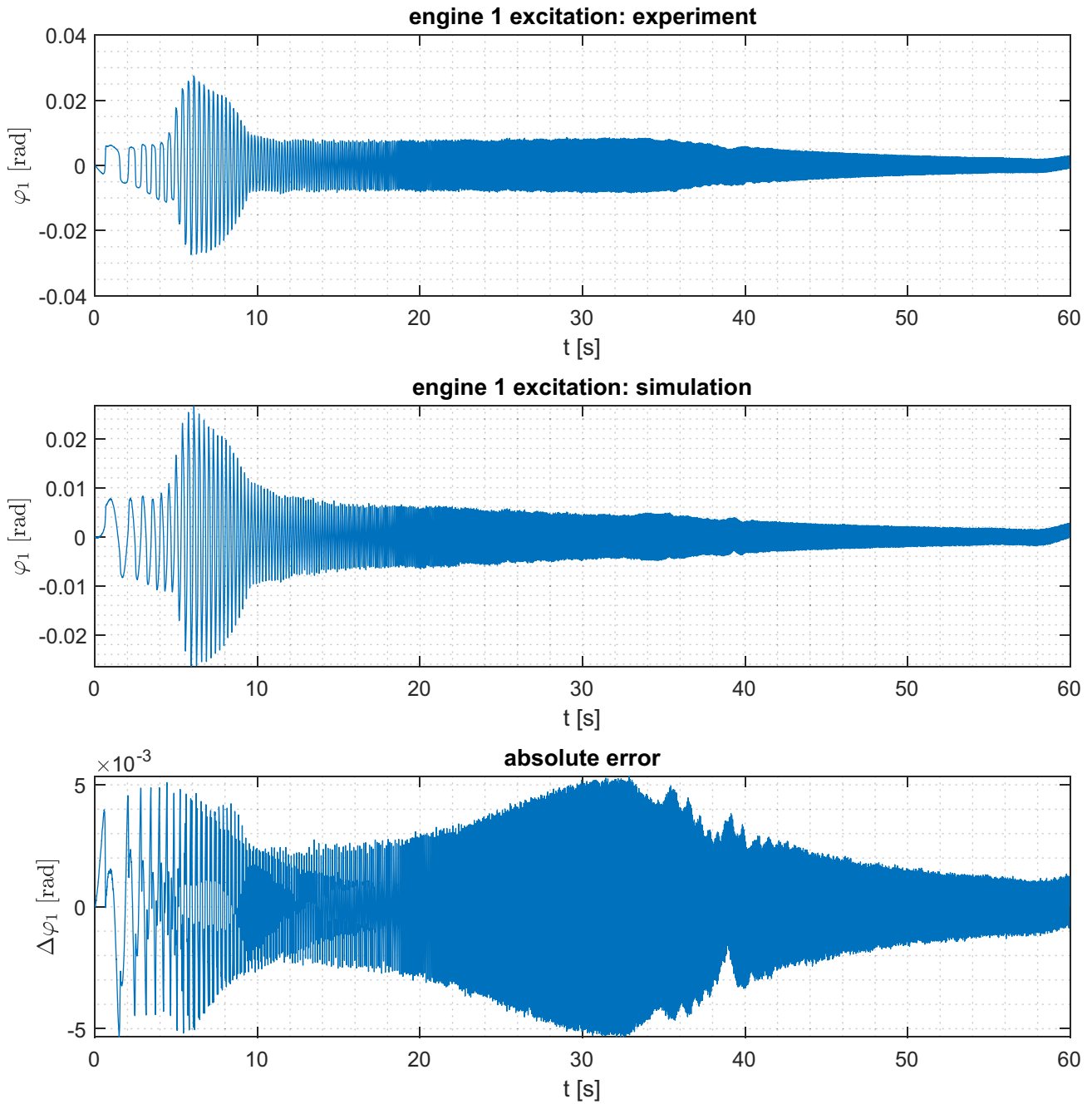
Vector of unknowns is solved using least squares method leading to pseudo inversion assembly.

$$
\begin{bmatrix} k_{t1} \\ I_1 \\ b_{M1} \\ k_{t2} \\ I_2 \\ b_{M2} \end{bmatrix} = \left(\mathbb{V}^T \mathbb{V} \right)^{-1} \mathbb{V}^T \mathbb{U}
\tag{23}
$$

Resulting moments of inertia $I_1 = 7.98 \cdot 10^{-4} kgm^2$, $I_2 = 8.74 \cdot 10^{-4} kgm^2$, current constants $k_{t1} = 0.15 \frac{Nm}{A}$, $k_{t2} = 0.2 \frac{Nm}{A}$, and

Fig. 9 Verification of identified model: motor parameters, motor 1 excitation

dampings $b_{M1} = 0.035 Nms$, $b_{M2} = 0.005 Nms$ are verified in the simulation experiment, where the Eq. (19) has currents i_1, i_2 and beam TCP position x_n as inputs. Comparisons of simulated rotor angular positions with measurement are at Figs. 9 and 10. Behaviour of motor 1 is at Fig. 9, and behaviour of motor 2 is at Fig. 10. The graphs show the experimental

(measured) data, then simulated data and their difference as absolute error. System drift at low frequencies (less than 0.3Hz) is subtracted.

The comparison in frequency domain is at Fig. 11. Left part shows behaviour of the first motor, right part shows the behaviour of the second motor.
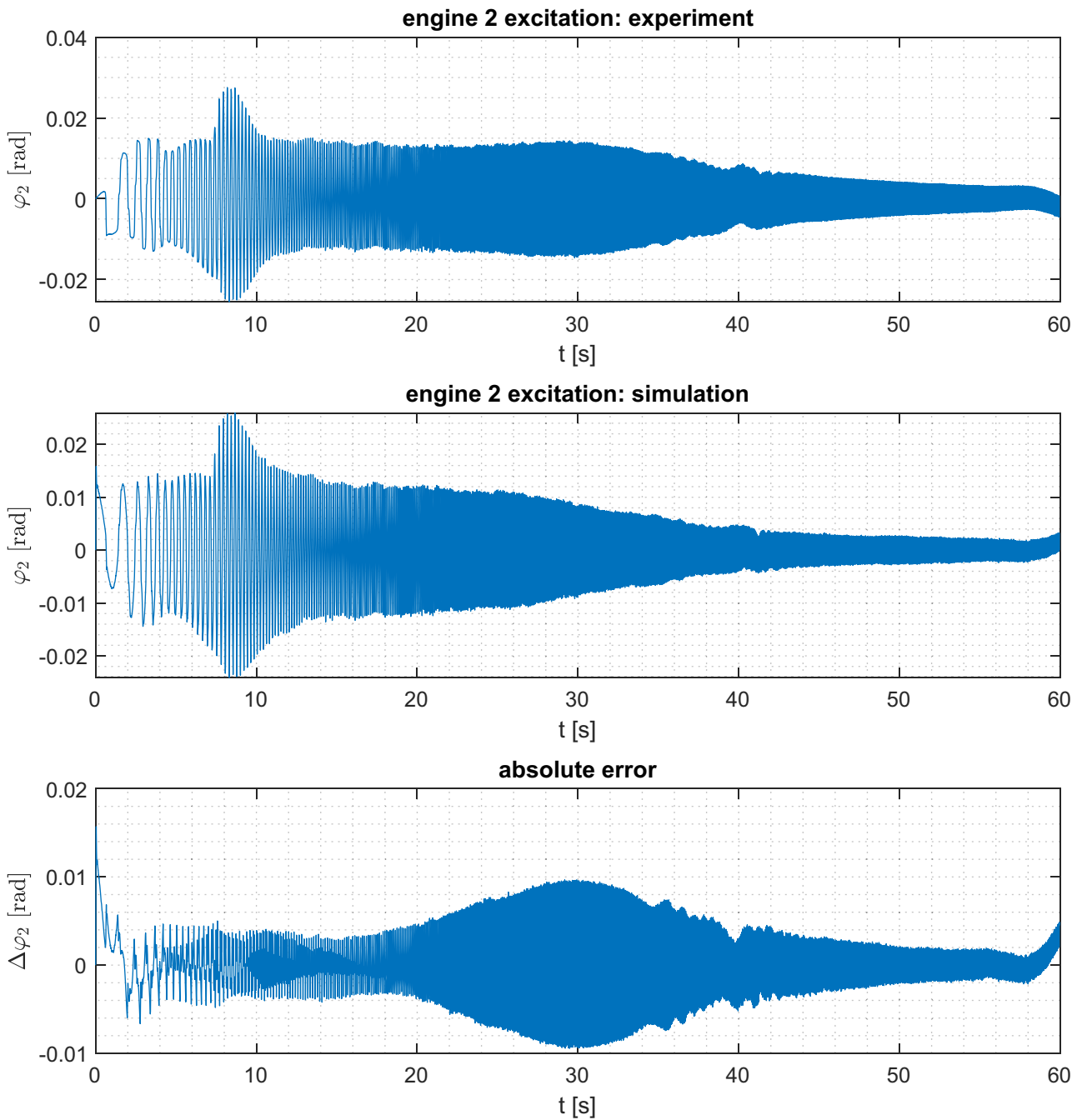
**Fig. 10** Verification of identified model: motor parameters, motor 2 excitation

2.2 System linearization

The set of Eq. (1) is linearized at the particular equilibrium operating point. The only nonlinear terms are in Eq. (4), the length L_1 and L_2 depend on variable x_n, and the same is for

angles α_1 and α_2. Horizontal displacement x_n is projected into the L_1 and L_2 directions as follows:

$$L_1 - L_{10} = x_n \cos \alpha_1$$
$$L_2 - L_{20} = -x_n \cos \alpha_2 \tag{24}$$

Fig. 11 Verification of identified model: motor parameters, frequency analysis
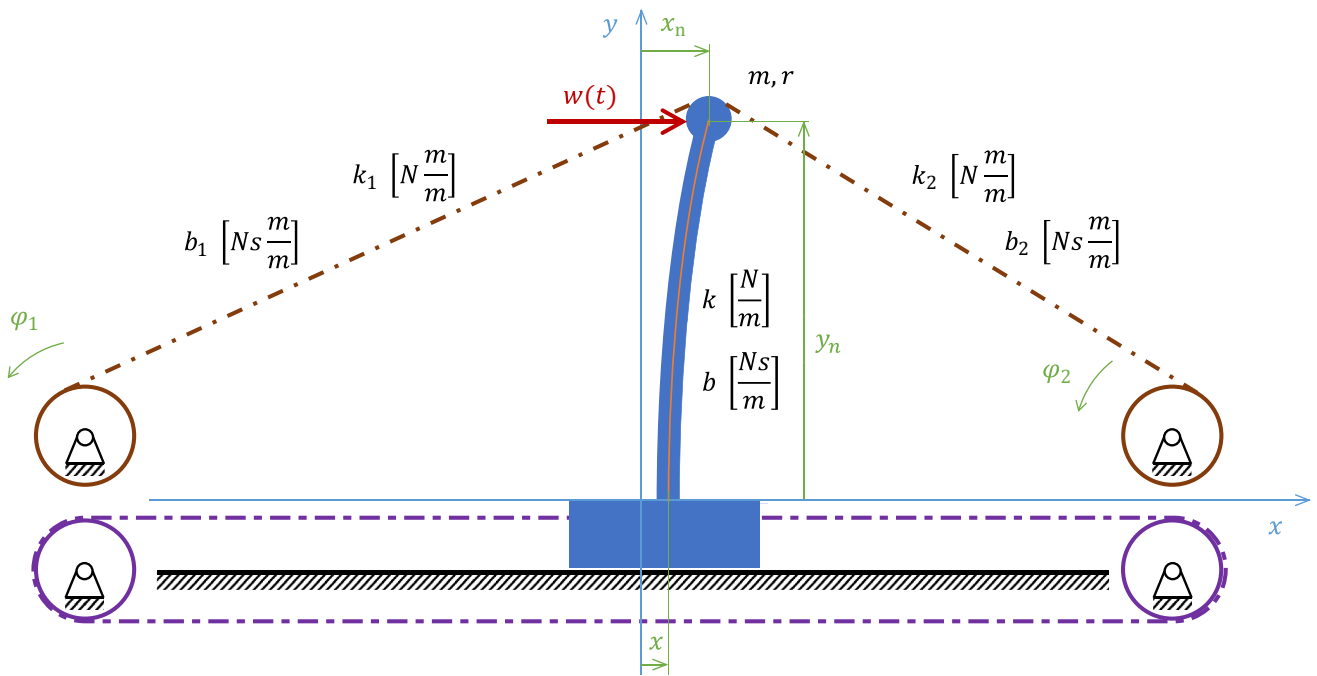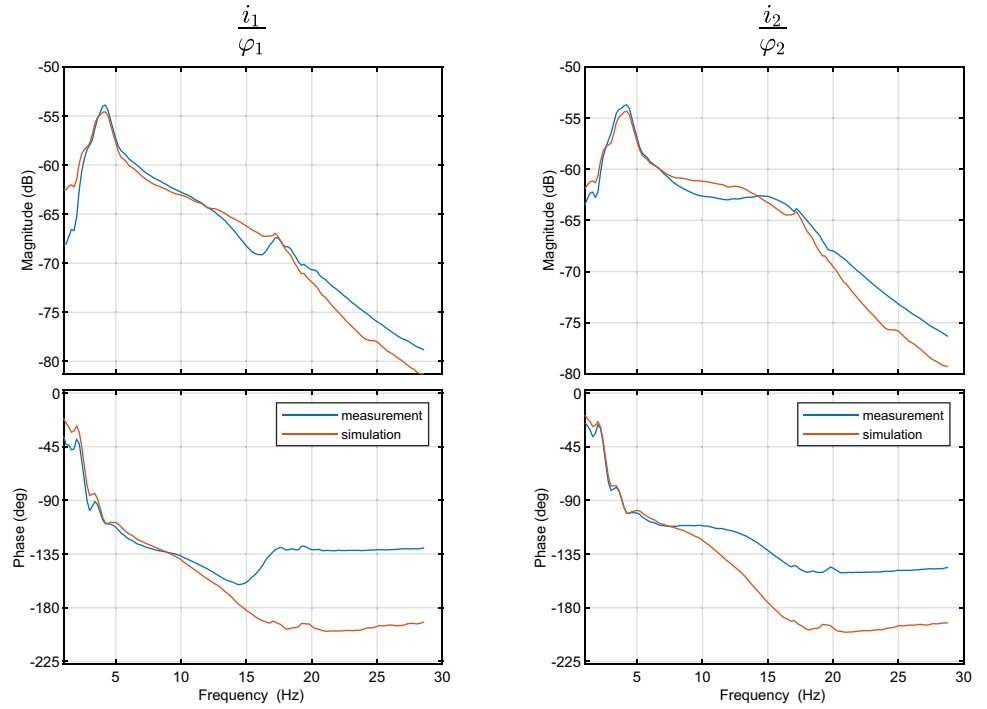
Fig. 12 Model with drives in position control mode (kinematic constraint is applied at angles φ_1 and φ_2) and applied external disturbance force w

while change in α_1 and α_2 due to the small x_n is neglected. Cable longitudinal deformation in Eq. (3) is further simplified:

$$\xi_1 = x_n \cos \alpha_1 + \varphi_1 r_1$$
$$\xi_2 = -x_n \cos \alpha_2 - \varphi_2 r_2 \tag{25}$$

The linearized system of eigen equations of motion is following:

$$I_1 \ddot{\varphi}_1 = i_1 k_{t1} - \frac{k_L r_1}{L_1}\left(x_n \cos \alpha_1 + \varphi_1 r_1\right) - \frac{b_L r_1}{L_1}\left(\dot{x}_n \cos \alpha_1 + \dot{\varphi}_1 r_1\right) - b_{M1}\dot{\varphi}_1$$

$$I_2 \ddot{\varphi}_2 = i_2 k_{t2} - \frac{k_L r_2}{L_2}\left(x_n \cos \alpha_2 + \varphi_2 r_2\right) - \frac{b_L r_2}{L_2}\left(\dot{x}_n \cos \alpha_2 + \dot{\varphi}_2 r_2\right) - b_{M2}\dot{\varphi}_2$$

$$m\ddot{x}_n = -k(x_n - x) - b(\dot{x}_n - \dot{x}) + \frac{k_L}{L_2}\left(-x_n \cos \alpha_2 - \varphi_2 r_2\right)\cos \alpha_2 +$$
$$+ \frac{b_L}{L_2}\left(-\dot{x}_n \cos \alpha_2 - \dot{\varphi}_2 r_2\right)\cos \alpha_2 - \frac{k_L}{L_1}\left(x_n \cos \alpha_1 + \varphi_1 r_1\right)\cos \alpha_1 -$$
$$- \frac{b_L}{L_1}\left(\dot{x}_n \cos \alpha_1 + \dot{\varphi}_1 r_1\right)\cos \alpha_1 \tag{26}$$

with inputs i_1, i_2 and cart coordinate x (with its time derivative $\dot{x}$).

3 Vibration damping analysis

The sensitivity of real mechanical systems to external disturbance determines their usefulness and suitability for particular task. Analysis and reduction of sensitivity are the main goal of this paper.

External disturbance with significant effect of given presented mechanical system (Fig. 1) is the horizontal force application on the beam tip (TCP). For evaluation of system vibration damping capability, the frequency analysis of the transfer function $\frac{Y}{W}$ is performed. W represents disturbance and Y system output, in the case of our system the disturbance is applied horizontal force and output is the horizontal coordinate of the beam tip, x_n.

The state-space representation is used for system properties evaluation. The comparison is performed also with the system without the cables. The state-space system description has the following form:

$$\dot{\mathbf{z}} = \mathbb{A}\mathbf{z} + \mathbb{B}\mathbf{u}$$
$$\mathbf{y} = \mathbb{C}\mathbf{z} + \mathbb{D}\mathbf{u} \tag{27}$$
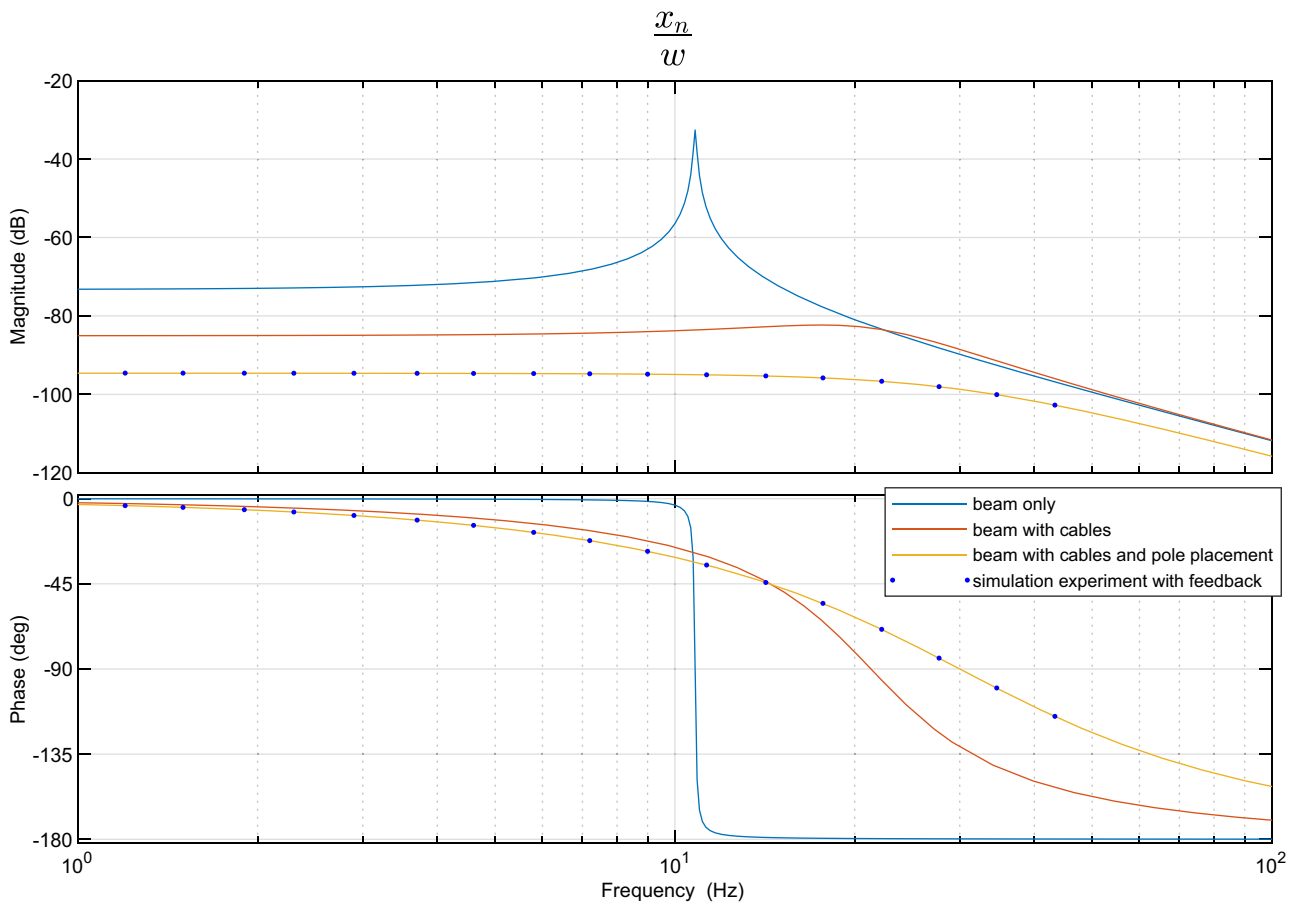
Fig. 13 Magnitude phase diagram of the transfer function $\frac{x_n}{w}$ is plotted, x_n is beam tip horizontal coordinate, and w is horizontal disturbance force applied at beam tip. There is performed the comparison between original beam structure (blue line) and structure with cables with drives in position control mode (without control — red line and with state feedback control — yellow line)

The state-space matrices for the system without cables excited by external force $w(t)$ as at Fig. 12 are the following:

$$\mathbb{A} = \begin{bmatrix} 0 & -\frac{k}{m} \\ 1 & -\frac{b}{m} \end{bmatrix} \qquad \mathbb{B} = \begin{bmatrix} \mathbb{B}_x & \mathbb{B}_w \end{bmatrix} \qquad \mathbb{B}_x = \begin{bmatrix} \frac{k}{m} \\ \frac{b}{m} \end{bmatrix} \qquad \mathbb{B}_w = \begin{bmatrix} \frac{1}{m} \\ 0 \end{bmatrix}$$

$$\mathbb{C} = \begin{bmatrix} 0 & 1 \end{bmatrix} \qquad \mathbb{D} = \begin{bmatrix} 0 & 0 \end{bmatrix}$$

(28)

The output is x_n coordinate, inputs are x and w:

$$\mathbf{z} = \begin{bmatrix} z_1 \\ z_2 \end{bmatrix} \qquad z_2 = x_n \qquad \mathbf{u} = \begin{bmatrix} x \\ w \end{bmatrix} \qquad \mathbf{y} = \begin{bmatrix} x_n \end{bmatrix}$$

(29)

The system is transformed into the Laplace domain and corresponding transfer function $\frac{X_n}{W}$ for the system without cables is

$$\frac{X_n}{W} = \mathbb{C}(\mathbb{I}s - \mathbb{A})^{-1}\mathbb{B}_w =$$

$$= \frac{1}{ms^2 + bs + k}$$

(30)

where symbol s represents Laplace variable, X_n and W are output (beam tip horizontal coordinate) and input (horizontal force) in the Laplace domain, and $\mathbb{I}$ represents eigenmatrix of the same size as matrix $\mathbb{A}$.

3.1 Effect of cables with drives in position control mode

The system with the cables and drives in position control mode with external disturbance force $w(t)$ is depicted at Fig. 12. If the drives are in position control mode, the prescribed drive positions form in fact the kinematic excitation. The system properties are compared with the system without cable structure.

The linearized equations describing the system in Fig. 12 are derived from Eq. (26), and only the third equation is used. For obtaining the frequency response, the state space representation is assembled.
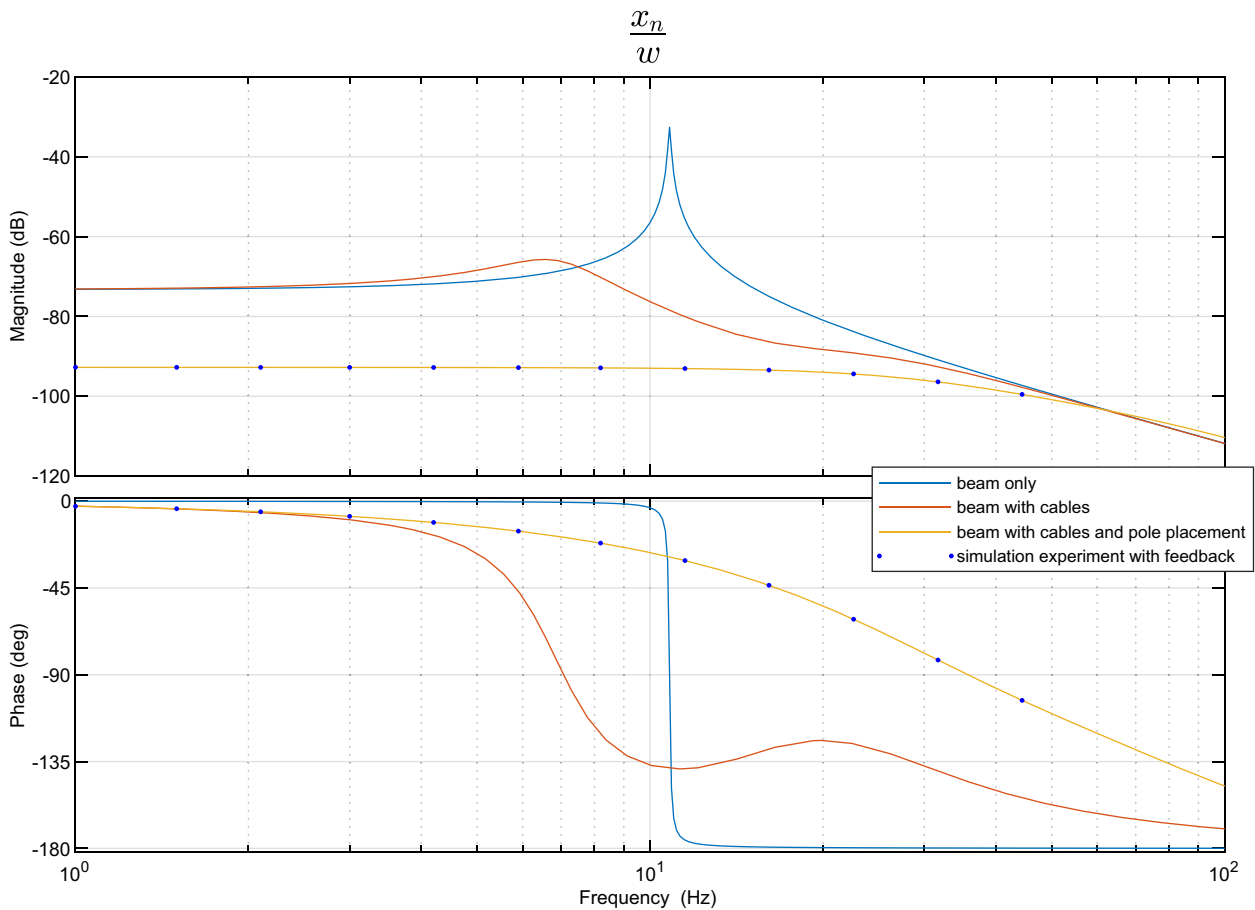
Fig. 14 Magnitude phase diagram of the transfer function $\frac{x_n}{w}$ is plotted, x_n is beam tip horizontal coordinate, and w is horizontal disturbance force applied at beam tip. There is performed the comparison between original beam structure (blue line) and structure with cables with electric drives in torque control mode (without control — red line and with state feedback control — yellow line)

$$
\mathbb{A}_1 = \begin{bmatrix} 0 & -\frac{1}{m}\left(k + \frac{k_L \cos^2 \alpha_1}{L_1} + \frac{k_L \cos^2 \alpha_2}{L_2}\right) \\ 1 & -\frac{1}{m}\left(b + \frac{b_L \cos^2 \alpha_1}{L_1} + \frac{b_L \cos^2 \alpha_2}{L_2}\right) \end{bmatrix}
$$

$$
\mathbb{B}_1 = \begin{bmatrix} \mathbb{B}_\varphi & \mathbb{B}_{x1} & \mathbb{B}_{w1} \end{bmatrix}
$$

$$
\mathbb{B}_\varphi = \begin{bmatrix} -\frac{k_L r_1 \cos \alpha_1}{mL_1} & -\frac{k_L r_2 \cos \alpha_2}{mL_2} \\ -\frac{b_L r_1 \cos \alpha_1}{mL_1} & -\frac{b_L r_2 \cos \alpha_2}{mL_2} \end{bmatrix} \quad \mathbb{B}_{x1} = \begin{bmatrix} \frac{k}{m} \\ \frac{b}{m} \end{bmatrix} \quad \mathbb{B}_{w1} = \begin{bmatrix} \frac{1}{m} \\ 0 \end{bmatrix}
$$

$$
\mathbb{C}_1 = \begin{bmatrix} 0 & 1 \end{bmatrix} \quad \mathbb{D}_1 = \begin{bmatrix} 0 & 0 & 0 & 0 \end{bmatrix}
$$

(31)

The output is x_n coordinate, and inputs are φ_1, φ_2, x, and w.

$$
\mathbf{z}_1 = \begin{bmatrix} z_{11} \\ z_{12} \end{bmatrix} \quad x_n = z_{12} \quad \mathbf{u}_1 = \begin{bmatrix} \varphi_1 \\ \varphi_2 \\ x \\ w \end{bmatrix} \quad \mathbf{y}_1 = \begin{bmatrix} x_n \end{bmatrix}
$$

(32)

The transfer function $\frac{X_n}{W}$ is

$$
\frac{X_n}{W} = \mathbb{C}_1 (\mathbb{I}s - \mathbb{A}_1)^{-1} \mathbb{B}_{w1} =
$$

$$
= \frac{1}{ms^2 + \left(b + \frac{b_L \cos^2 \alpha_1}{L_1} + \frac{b_L \cos^2 \alpha_2}{L_2}\right)s + k + \frac{k_L \cos^2 \alpha_1}{L_1} + \frac{k_L \cos^2 \alpha_2}{L_2}}
$$

(33)

The original system (without cables) has eigenfrequency $10.81Hz$ and damping $\zeta = 4.6 \cdot 10^{-3}$, system with cables has eigenfrequency $21.27Hz$ with $\zeta = 0.4$, and we are going to introduce the state feedback control with damped arbitrarily prescribed poles ($\Omega = 30Hz$ and $\zeta = 0.8$) using pole placement algorithm [46]. The system $(\mathbb{A}_1, \mathbb{B}_\varphi)$ is controllable and feedback gain $\mathbb{K}_{place1}$ is obtained. The transfer function of controlled system Eq. (34) is investigated too.

$$
\frac{X_n}{W} = \mathbb{C}_1 (\mathbb{I}s - (\mathbb{A}_1 - \mathbb{B}_\varphi \mathbb{K}_{place1}))^{-1} \mathbb{B}_{w1}
$$

(34)

The comparison of external disturbance sensitivity is shown at Fig. 13. System extended with cables move the overall eigenfrequency and its behaviour is in comparison with original structure more damped. If we use the state feedback to choose the eigenfrequency and adequate damping, the sensitivity to disturbance further decreases.

The simulation experiment is performed too and it verifies the findings. The system with and without cables is loaded with disturbance force at different frequencies (sweep cosine function is used) to obtain the $\frac{x_n}{w}$ transfer function behaviour. At Fig. 13, the dotted line represents the simulation experiment verification of system with pole placement.

3.2 Effect of cables with drives in torque control mode

The full model of experimental stand on Fig. 2 excited at beam tip with external horizontal force $w(t)$ as disturbance is investigated. The system with cables is compared with the system without cable structure, which is common with the previous case.

The linearized equations at Eq. (26) are used for assorting the state space representation. It further serves as a base for the system frequency response.

$$
\mathbb{A}_2 = \begin{bmatrix} 0 & -\frac{1}{m}\left(k + \frac{k_L \cos^2 \alpha_1}{L_1} + \frac{k_L \cos^2 \alpha_2}{L_2}\right) & 0 & -\frac{k_L r_1 \cos \alpha_1}{I_1 L_1} & 0 & -\frac{k_L r_2 \cos \alpha_2}{I_2 L_2} \\ 1 & -\frac{1}{m}\left(b + \frac{b_L \cos^2 \alpha_1}{L_1} + \frac{b_L \cos^2 \alpha_2}{L_2}\right) & 0 & -\frac{b_L r_1 \cos \alpha_1}{I_1 L_1} & 0 & -\frac{b_L r_2 \cos \alpha_2}{I_2 L_2} \\ 0 & -\frac{k_L r_1 \cos \alpha_1}{mL_1} & 0 & -\frac{k_L r_1^2}{I_1 L_1} & 0 & 0 \\ 0 & -\frac{b_L r_1 \cos \alpha_1}{mL_1} & 1 & -\frac{b_{M1}}{I_1} - \frac{b_L r_1^2}{I_1 L_1} & 0 & 0 \\ 0 & -\frac{k_L r_2 \cos \alpha_2}{mL_2} & 0 & 0 & 0 & -\frac{k_L r_2^2}{I_2 L_2} \\ 0 & -\frac{b_L r_2 \cos \alpha_2}{mL_2} & 0 & 0 & 1 & -\frac{b_{M2}}{I_2} - \frac{b_L r_2^2}{I_2 L_2} \end{bmatrix}
$$

$$
\mathbb{B}_2 = \begin{bmatrix} \mathbb{B}_i & \mathbb{B}_{x2} & \mathbb{B}_{w2} \end{bmatrix}
$$

$$
\mathbb{B}_i = \begin{bmatrix} 0 & 0 \\ 0 & 0 \\ k_{t1} & 0 \\ 0 & 0 \\ 0 & k_{t2} \\ 0 & 0 \end{bmatrix} \quad \mathbb{B}_{x2} = \begin{bmatrix} k \\ b \\ 0 \\ 0 \\ 0 \\ 0 \end{bmatrix} \quad \mathbb{B}_{w2} = \begin{bmatrix} 1 \\ 0 \\ 0 \\ 0 \\ 0 \\ 0 \end{bmatrix}
$$

$$
\mathbb{C}_2 = \begin{bmatrix} 0 & \frac{1}{m} & 0 & 0 & 0 & 0 \end{bmatrix} \quad \mathbb{D}_2 = \begin{bmatrix} 0 & 0 & 0 & 0 \end{bmatrix}
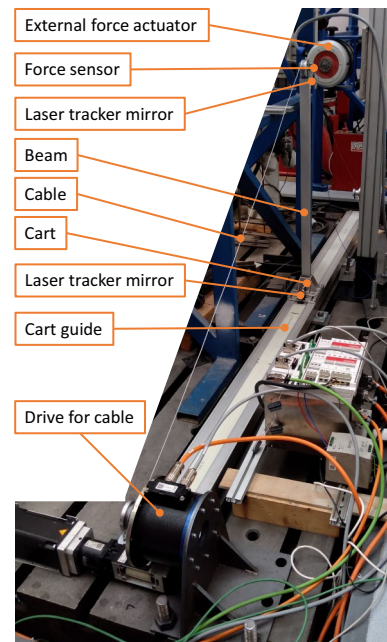$$

(35)

Fig. 15 Experimental stand description

The output is x_n coordinate, inputs are electric drive currents i_1 and i_2, cart coordinate x, and external force w.

$$\mathbf{z}_2 = \begin{bmatrix} z_{21} \\ z_{22} \\ z_{23} \\ z_{24} \\ z_{25} \\ z_{26} \end{bmatrix} \quad x_n = \frac{z_{22}}{m} \quad \varphi_1 = \frac{z_{24}}{I_1} \quad \varphi_2 = \frac{z_{26}}{I_2} \quad \mathbf{u}_2 = \begin{bmatrix} i_1 \\ i_2 \\ x \\ w \end{bmatrix} \quad \mathbf{y}_2 = \begin{bmatrix} x_n \end{bmatrix}$$

(36)

The transfer function $\frac{X_n}{W}$ as a measure of vibration damping is

$$\frac{X_n}{W} = \mathbb{C}_2 \left(\mathbb{I}s - \mathbb{A}_2 \right)^{-1} \mathbb{B}_{w2} =$$
$$= \frac{c_4 s^4 + c_3 s^3 + c_2 s^2 + c_1 s + c_0}{s^6 + a_5 s^5 + a_4 s^4 + a_3 s^3 + a_2 s^2 + a_1 s + a_0}$$

(37)

where coefficients $a_0, ..., a_5$ and $c_0, ..., c_4$ are in the Appendix section.

The model with drives and cables has three eigenfrequencies: 6.87Hz with damping 0.2, 15.78Hz with damping 0.5, and 24.95Hz with damping 0.6. The first eigenfrequency, which appears due to the electric drives equations of motion, is danger one, because of the relatively small damping. The behaviour of the system at Fig. 14 affirms the suspect. That is the reason to introduce state feedback control as in the previous case. The system $\left(\mathbb{A}_2, \mathbb{B}_i \right)$ is controllable and feedback gain $\mathbb{K}_{place2}$ is calculated. The prescribed poles with arbitrarily prescribed frequencies are 30Hz, 80Hz, and 90Hz with common damping 0.8. The transfer function of controlled system is the following:

$$\frac{X_n}{W} = \mathbb{C}_2 \left(\mathbb{I}s - \left(\mathbb{A}_2 - \mathbb{B}_i \mathbb{K}_{place2} \right) \right)^{-1} \mathbb{B}_{w2}$$

(38)
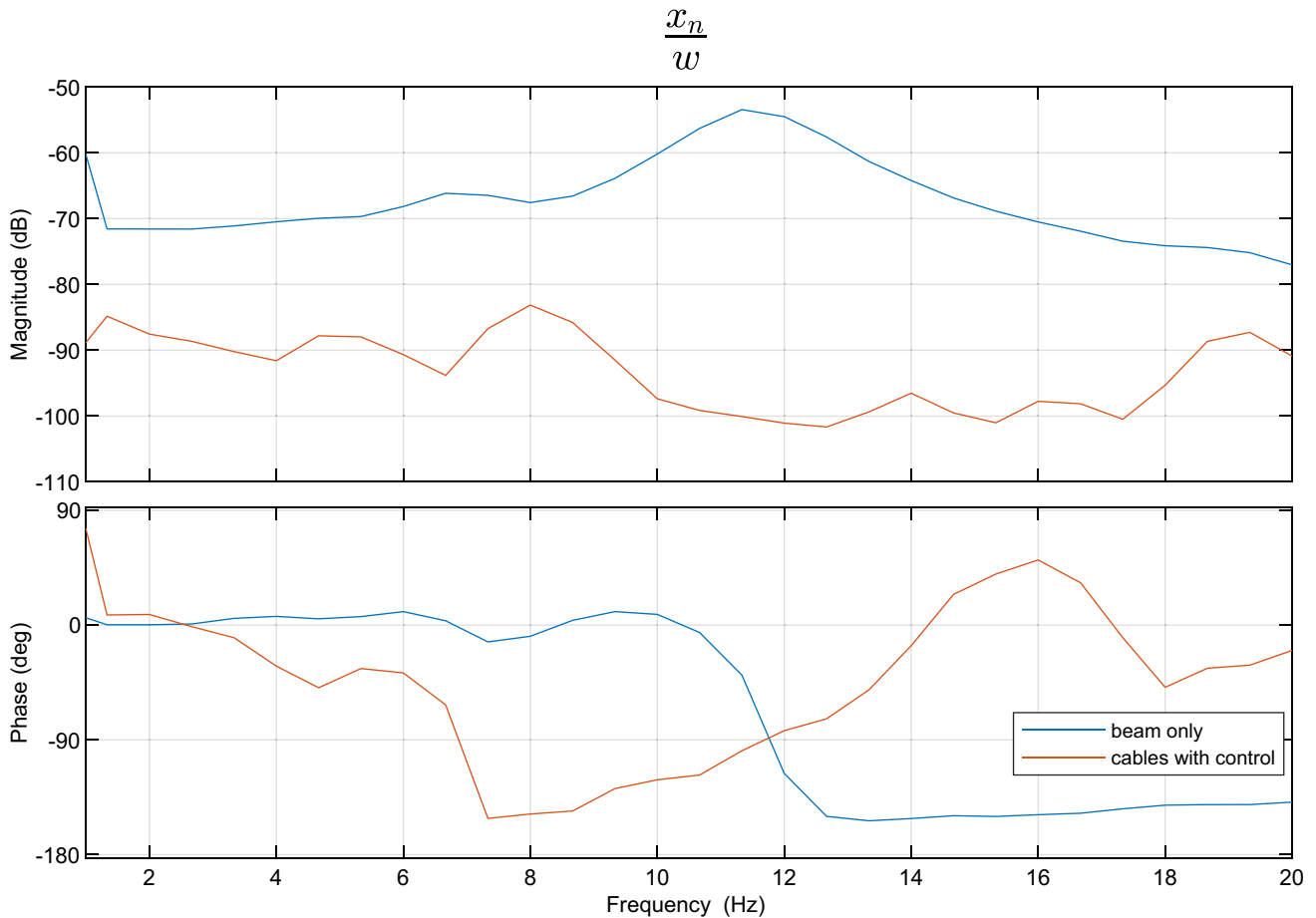
Fig. 16 Magnitude phase diagram of the transfer function $\frac{x_n}{w}$ is plotted, x_n is measured beam tip horizontal position, and w is horizontal disturbance force measured at beam tip. The comparison between original beam structure (blue line) and structure with cables with preload torque and feedback control (red line)

The transfer function $\frac{x_n}{w}$ behaviour as a measure of system sensitivity to external disturbances is shown at Fig. 14. System extended with cables has similar behaviour as the original system at low frequencies, but newly arises the first eigenfrequency and the feedback in this region is needed to improve the system vibration suppression properties.

Similarly as in the first case, the simulation experiment is performed and it verifies the findings. At Fig. 14, the dotted line represents some of the simulation experiment points.

4 Experimental test

The experimental verification of proposed cable system is performed. The setup is described in Fig. 15.

The mechanical system consists of the cart mounted to linear axis Rexroth with the electric drive Kollmorgen 6SM 57M-3.000-S3-1325. On the cart is mounted a beam with the cables attached at its tip. The cables are actuated with electric drives Kollmorgen D062M-92-9310-010. The cart and beam tip horizontal positions are measured by lasertracker Leica AT960-MR and Leica AT901-B, respectively, and the drive angular positions are measured by internal sensors. The whole system is managed by real-time control system Beckhoff AX5911 TwinCAT3 based on bus EtherCAT. The horizontal external force at the beam tip is excited by shaker Tira TV51140 and measured by force sensor PCB Piezotronics 208C02 connected to the Brüel &Kjaer 2694 amplifier.

The external horizontal force, as a disturbance, is set to be sweep cosine function with frequency change from 0.5 until 20Hz. The force magnitude is tuned manually.

Measurement result with feedback control algorithm shows the transfer function $\frac{x_n}{w}$ at Fig. 16. The feedback gain is obtained in a similar way as for Eq. (38) with prescribed frequencies 30Hz, 35Hz, and 40Hz and common damping 0.5; the condition of always loaded cables is fulfilled by demanded torque modification. The cable structure with applied feedback control decreases the system sensitivity to the external disturbance up to $-20dB$ and the system eigenfrequency is not significantly excited.

5 Conclusions

Vibration suppression is frequently solved in engineering practice. The presented approach deals with the flexible structure and such systems are often problematic. The flexibility does not allow higher dynamic movements without residual vibrations. To overcome this problem, the auxiliary cable structure is attached to the system to increase system stiffness and remove the oscillations.

The resonance amplitude of the plant was suppressed and behaviour of the system until 15Hz was reduced by $-20dB$ using the cable structure with feedback control. It was shown that the concept is suitable to be used for vibration damping of slender structures.

Obtained results conceptionaly prove the validity of proposed concept. Follow-up research will deal with deeper experimental verification of the achieved results.

The obtained results can be summarized as follows:

- Experimental stand representing the main properties of machine tools with a large workspace and long and heavy movable parts damped by auxiliary cable structure is prepared
- The cables can be easily reconfigured and the original workspace of machine is almost preserved
- Experimental stand identification is performed and model is created
- State feedback simplified model control law for cable structure is assembled
- Frequency analysis shows the vibration suppression
- Low frequencies are suppressed, especially first eigenfrequency
- Additional cable system uses standard drives commonly used by machine tool manufacturers
- Experimental test shows the desired behaviour with transfer function reduction of 20dB

Appendix

Coefficients of transfer function in (37) are the following:

$$c_4 = \frac{1}{m}$$

$$c_3 = \frac{b_L}{m}\left(\frac{r_1^2}{I_1 L_1} + \frac{r_2^2}{I_2 L_2}\right) + \frac{b_{M1}}{I_1 m} + \frac{b_{M2}}{I_2 m}$$

$$c_2 = \frac{b_L}{m}\left(\frac{b_L r_1^2 r_2^2}{I_1 I_2 L_1 L_2} + \frac{b_{M2} r_1^2}{I_1 I_2 L_1} + \frac{b_{M1} r_2^2}{I_1 I_2 L_2}\right) + \frac{k_L}{m}\left(\frac{r_1^2}{I_1 L_1} + \frac{r_2^2}{I_2 L_2} + \frac{b_{M1} b_{M2}}{I_1 I_2 m}\right)$$

$$c_1 = \frac{k_L}{m}\left(\frac{2b_L r_1^2 r_2^2}{I_1 I_2 L_1 L_2} + \frac{b_{M2} r_1^2}{I_1 I_2 L_1} + \frac{b_{M1} r_2^2}{I_1 I_2 L_2}\right)$$

$$c_0 = \frac{k_L}{m}\frac{k_L r_1^2 r_2^2}{I_1 I_2 L_1 L_2}$$

$$a_5 = \frac{b_{M1}}{I_1} + \frac{b_{M2}}{I_2} + \frac{b}{m} + b_L\left(\frac{r_1^2}{I_1 L_1} + \frac{r_2^2}{I_2 L_2} + \frac{\cos^2\alpha_1}{L_1 m} + \frac{\cos^2\alpha_2}{L_2 m}\right)$$

$$a_4 = \frac{k}{m} + \left(k_L + \frac{b}{m}b_L\right)\left(\frac{r_1^2}{I_1 L_1} + \frac{r_2^2}{I_2 L_2}\right) + \frac{b_{M1}b_{M2}}{I_1 I_2} + \frac{b}{m}\left(\frac{b_{M1}}{I_1} + \frac{b_{M2}}{I_2}\right) +$$

$$+ \frac{b_L}{I_1 I_2}\left(\frac{b_{M2}r_1^2}{L_1} + \frac{b_{M1}r_2^2}{L_2} + \frac{b_L r_1^2 r_2^2}{L_1 L_2}\right) +$$

$$+ \frac{\cos^2\alpha_1}{m L_1}\left(k_L + \frac{b_L^2 r_2^2}{I_2 L_2} + \frac{b_L b_{M1}}{I_1} + \frac{b_L b_{M2}}{I_2}\right) +$$

$$+ \frac{\cos^2\alpha_2}{m L_2}\left(k_L + \frac{b_L^2 r_1^2}{I_1 L_2} + \frac{b_L b_{M1}}{I_1} + \frac{b_L b_{M2}}{I_2}\right)$$

$$a_3 = \frac{k}{m}\left(\frac{b_{M1}}{I_1} + \frac{b_{M2}}{I_2} + \frac{b_L r_1^2}{I_1 L_1} + \frac{b_L r_2^2}{I_2 L_2}\right) +$$

$$+ \frac{b}{m}\left(\frac{k_L r_1^2}{I_1 L_1} + \frac{k_L r_2^2}{I_2 L_2} + \frac{b_{M1}b_{M2}}{I_1 I_2} + \frac{b_L b_{M2}r_1^2}{I_1 I_2 L_1}\right) +$$

$$+ \frac{b_{M2}k_L r_1^2}{I_1 I_2 L_1} + \frac{b_{M1}r_2^2}{I_1 I_2}\left(\frac{k_L}{L_2} + \frac{b_L b}{L_2 m}\right) + \frac{r_1^2 r_2^2}{I_1 I_2 L_1}\left(\frac{2b_L k_L}{L_2} + \frac{b b_L}{L_2 m}\right) +$$

$$+ \frac{\cos^2\alpha_1}{L_1 m}\left(\frac{k_L}{I_2}\left(b_{M2} + \frac{2b_L r_2^2}{L_2}\right) + \frac{b_{M1}}{I_1}\left(\frac{b_L^2 r_2^2}{I_2 L_2} + \frac{b_L b_{M2}}{I_2} + k_L\right)\right) +$$

$$+ \frac{\cos^2\alpha_2}{L_2 m}\left(\frac{b_{M2}}{I_2}\left(\frac{b_L^2 r_1^2}{I_1 L_1} + \frac{b_L b_{M1}}{I_1} + k_L\right) + \frac{k_L}{I_1}\left(\frac{2b_L r_1^2}{L_1} + b_{M1}\right)\right)$$

$$a_2 = \frac{k}{m}\left(\frac{k_L r_1^2}{I_1 L_1} + \frac{k_L r_2^2}{I_2 L_2} + \frac{b_{M1}b_{M2}}{I_1 I_2}\right) + \frac{r_1^2 r_2^2}{I_1 I_2}\left(\frac{k_L^2}{L_1 L_2} + \frac{b_L^2 k}{L_1 L_2 m} + \frac{2bk_L b_L}{L_1 L_2 m}\right) +$$

$$+ \frac{k_L \cos^2\alpha_1}{I_2 L_1 m}\left(\frac{2b_L b_{M1}r_2^2}{I_1 L_2} + \frac{b_{M1}b_{M2}}{I_1} + \frac{k_L r_2^2}{L_2}\right) +$$

$$+ \frac{k_L \cos^2\alpha_2}{I_1 L_2 m}\left(\frac{2b_L b_{M2}r_1^2}{I_2 L_1} + \frac{b_{M1}b_{M2}}{I_2} + \frac{k_L r_1^2}{L_1}\right) +$$

$$+ \left(\frac{bk_L}{I_1 m} + \frac{b_L k}{I_1 m}\right)\left(\frac{b_{M1}r_2^2}{I_2 L_2} + \frac{b_{M2}r_1^2}{I_2 L_1}\right)$$

$$a_1 = \frac{k_L}{I_1 m}\left(\frac{b_{M2}r_1^2}{I_2 L_1} + \frac{b_{M1}r_2^2}{I_2 L_2} + \frac{2b_L r_1^2 r_2^2}{I_2 L_1 L_2}\right) +$$

$$+ \frac{k_L^2}{I_1}\left(\frac{b_{M1}r_2^2\cos^2\alpha_1}{I_2 L_1 L_2 m} + \frac{b_{M2}r_1^2\cos^2\alpha_2}{I_2 L_1 L_2 m} + \frac{b r_1^2 r_2^2}{I_2 L_1 L_2 m}\right)$$

$$a_0 = \frac{k k_L^2 r_1^2 r_2^2}{I_1 I_2 L_1 L_2 m}$$

Declarations

Consent to participate Not applicable.

Consent for publication Not applicable.

Competing interests The authors declare no competing interests.

References

1. Yang Y, Xie R, Liu Q (2017) Design of a passive damper with tunable stiffness and its application in thin-walled part milling. Int J Adv Manuf Technol 89(9–12):2713–2720. https://doi.org/10.1007/s00170-016-9474-7

2. Samani FS, Pellicano F (2012) Vibration reduction of beams under successive traveling loads by means of linear and nonlinear dynamic absorbers. J Sound Vib 331(10):2272–2290. https://doi.org/10.1016/j.jsv.2012.01.002

3. Šika Z (2004) Aktivní a poloaktivní snižování mechanického kmitání strojů. Habilitační práce, CTU in Prague, Prague

4. Kraus K, Šika Z, Beneš P, Krivošej J, Vyhlídal T (2020) Mechatronic robot arm with active vibration absorbers. J Vib Control 26(13–14):1145–1156. https://doi.org/10.1177/1077546320918488

5. Jenkins R, Olgac N (2019) Real-time tuning of delayed resonator-based absorbers for spectral and spatial variations. J Vib Acoust 141(2). https://doi.org/10.1115/1.4041592

6. Kammer AS, Olgac N (2016) Delayed resonator concept for vibration suppression using piezoelectric networks. Smart Mater Struct 25(11):115008. https://doi.org/10.1088/0964-1726/25/11/115008

7. Vyhlídal T, Olgac N, Kučera V (2014) Delayed resonator with acceleration feedback - complete stability analysis by spectral methods and vibration absorber design. J Sound Vib 333(25):6781–6795. https://doi.org/10.1016/j.jsv.2014.08.002

8. Vyhlídal T, Pilbauer D, Alikoç B, Michiels W (2019) Analysis and design aspects of delayed resonator absorber with position, velocity or acceleration feedback. J Sound Vib 459:114831. https://doi.org/10.1016/j.jsv.2019.06.038

9. Valášek M, Olgac N, Neusser Z (2019) Real-time tunable single-degree of freedom, multiple-frequency vibration absorber. Mech Syst Signal Process 133:106244. https://doi.org/10.1016/j.ymssp.2019.07.025

10. Valasek M, Olgac N, Neusser Z (2019) Exploring operational frequency ranges for actively-tuned single-mass, multiple-frequency vibration absorber. 2019 5th Indian Control Conference, ICC 2019 - Proceedings, pp 448–453. https://doi.org/10.1109/INDIANCC.2019.8715571

11. Šika Z, Vyhlídal T, Neusser Z (2021) Two-dimensional delayed resonator for entire vibration absorption. J Sound Vib 500:116010. https://doi.org/10.1016/j.jsv.2021.116010

12. Vyhlídal T, Michiels W, Neusser Z, Bušek J, Šika Z (2022) Analysis and optimized design of an actively controlled two-dimensional delayed resonator. Mech Syst Signal Process 178. https://doi.org/10.1016/j.ymssp.2022.109195

13. Neusser Z, Valášek M (2013) Control of the double inverted pendulum on a cart using the natural motion. Acta Polytechnica 53(6):883–889. https://doi.org/10.14311/AP.2013.53.0883

14. Neusser Z, Nečas M, Valášek M (2022) Control of flexible robot by harmonic functions. Appl Sci (Switzerland) 12(7). https://doi.org/10.3390/app12073604

15. Brecher C, Manoharan D, Ladra U, Köpken HG (2010) Chatter suppression with an active workpiece holder. Prod Eng 4(2–3):239–245. https://doi.org/10.1007/s11740-009-0204-y

16. Chen F, Lu X, Altintas Y (2014) A novel magnetic actuator design for active damping of machining tools. Int J Mach Tools Manuf 85:58–69. https://doi.org/10.1016/j.ijmachtools.2014.05.004

17. Xia Y, Wan Y, Luo X, Wang H, Gong N, Cao J, Liu Z, Song Q (2020) Development of a toolholder with high dynamic stiffness for mitigating chatter and improving machining efficiency in face milling. Mech Syst Signal Process 145:106928. https://doi.org/10.1016/j.ymssp.2020.106928

18. Yang Y, Wang Y, Liu Q (2019) Design of a milling cutter with large length-diameter ratio based on embedded passive damper. J Vib Control 25(3):506–516. https://doi.org/10.1177/1077546318786594

19. Ghorbani S, Rogov VA, Carluccio A, Belov PS (2019) The effect of composite boring bars on vibration in machining process. Int J Adv Manuf Technol 105(1–4):1157–1174. https://doi.org/10.1007/s00170-019-04298-6

20. Liu X, Liu Q, Wu S, Liu L, Gao H (2017) Research on the performance of damping boring bar with a variable stiffness dynamic vibration absorber. Int J Adv Manuf Technol 89(9–12):2893–2906. https://doi.org/10.1007/s00170-016-9612-2

21. Ma G, Xu M, Zhang S, Zhang Y, Liu X (2018) Active vibration control of an axially moving cantilever structure using PZT actuator. J Aerosp Eng 31(5):04018049. https://doi.org/10.1061/(ASCE)AS.1943-5525.0000853

22. Sajedi Pour D, Behbahani S (2016) Semi-active fuzzy control of machine tool chatter vibration using smart MR dampers. Int J Adv Manuf Technol 83(1–4):421–428. https://doi.org/10.1007/s00170-015-7503-6

23. Halamka V, Moravec J, Beneš P, Neusser Z, Koubek J, Kozlok T, Valášek M, Šika Z (2021) Drive axis controller optimization of production machines based on dynamic models. Int J Adv Manuf Technol 115(4):1277–1293. https://doi.org/10.1007/s00170-021-07160-w

24. Beneš P, Valášek M, Šika Z, Zavřel J, Pelikán J (2019) Shavo control: the combination of the adjusted command shaping and feedback control for vibration suppression. Acta Mech 230(5):1891–1905. https://doi.org/10.1007/s00707-019-2363-z

25. Liu Q, Lu H, Zhang X, Qiao Y, Cheng Q, Zhang Y, Wang Y (2020) A non-delay error compensation method for dual-driving gantry-type machine tool. Processes 8(7):748. https://doi.org/10.3390/pr8070748

26. Huang Y, Liu Z, Du R, Tang H (2019) Simulation and experiments of active vibration control for ultra-long flexible manipulator under impact loads. J Vib Control 25(3):675–684. https://doi.org/10.1177/1077546318794222

27. Alhazza KA, Majeed MA (2012) Free vibrations control of a cantilever beam using combined time delay feedback. J Vib Control 18(5):609–621. https://doi.org/10.1177/1077546311405700

28. Peng J, Zhang G, Xiang M, Sun H, Wang X, Xie X (2019) Vibration control for the nonlinear resonant response of a piezoelectric elastic beam via time-delayed feedback. Smart Mater Struct 28(9):095010. https://doi.org/10.1088/1361-665X/ab2e3d

29. Zl Zhao, Zc Qiu, Xm Zhang, Han Jd (2016) Vibration control of a pneumatic driven piezoelectric flexible manipulator using self-organizing map based multiple models. Mech Syst Signal Process 70–71:345–372. https://doi.org/10.1016/j.ymssp.2015.09.041

30. Cong Y, Kang H, Yan G (2021) Investigation of dynamic behavior of a cable-stayed cantilever beam under two-frequency excitations. Int J Non Linear Mech 129:103670. https://doi.org/10.1016/j.ijnonlinmec.2021.103670

31. Jalali MH, Rideout G (2019) Analytical and experimental investigation of cable-beam system dynamics. J Vib Control 25(19–20):2678–2691. https://doi.org/10.1177/1077546319867171

32. Huang YX, Tian H, Zhao Y (2016) Effects of cable on the dynamics of a cantilever beam with tip mass. Shock Vib 2016:1–10. https://doi.org/10.1155/2016/7698729

33. Tang L, Gouttefarde M, Sun H, Yin L, Zhou C (2021) Dynamic modelling and vibration suppression of a single-link flexible manipulator with two cables. Mech Mach Theory 162:104347. https://doi.org/10.1016/j.mechmachtheory.2021.104347

34. Holland DB, Virgin LN, Plaut RH (2008) Large deflections and vibration of a tapered cantilever pulled at its tip by a cable. J Sound Vib 310(1–2):433–441. https://doi.org/10.1016/j.jsv.2007.06.075

35. Sohn JW, Han YM, Choi SB, Lee YS, Han MS (2009) Vibration and position tracking control of a flexible beam using SMA wire actuators. J Vib Control 15(2):263–281. https://doi.org/10.1177/1077546308094251

36. Polach P, Hajžman M, Bulín R (2020) Modelling of dynamic behaviour of fibres and cables. In: Engineering Mechanics 2020, Institute of Thermomechanics of the Czech Academy of Sciences, Prague, Engineering Mechanics, pp 34–43. https://doi.org/10.21495/5896-3-034

37. Polach P, Byrtus M, Šika Z, Hajžman M (2017) Fibre spring-damper computational models in a laboratory mechanical system and validation with experimental measurement. The Interdisciplinary Journal of Discontinuity, Nonlinearity, and Complexity 6(4):513–523. https://doi.org/10.5890/DNC.2017.12.009

38. Polach P, Hajžman M, Dupal J (2017) Influence of the fibre damping computational model in a mechanical system on the coincidence with the experimental measurement results. Eng Rev 37(1):82–91

39. Polach P, Hajžman M, Šika Z, Červená O, Svatoš P (2014) Influence of the mass of the weight on the dynamic response of the asymmetric laboratory fibre-driven mechanical system. Applied and Computational Mechanics 8(1):75–90

40. Xiong H, Diao X (2020) Stiffness analysis of cable-driven parallel mechanisms with cables having large sustainable strains. Proceedings of the Institution of Mechanical Engineers, Part C: Journal of Mechanical Engineering Science 234(10):1959–1968. https://doi.org/10.1177/0954406220902165

41. Jiang X, Li B, Mao X, Mao K (2017) The multimode frequency analysis and its effect on the position accuracy of the sorting arm during operation. Adv Mech Eng 9(11):168781401772470. https://doi.org/10.1177/1687814017724703

42. Sun H, Hou S, Li Q, Tang X (2021) Research on the configuration of cable-driven parallel robots for vibration suppression of spatial flexible structures. Aerosp Sci Technol 109:106434. https://doi.org/10.1016/j.ast.2020.106434

43. Babaghasabha R, Khosravi MA, Taghirad HD (2015) Adaptive robust control of fully-constrained cable driven parallel robots. Mechatronics 25:27–36. https://doi.org/10.1016/j.mechatronics.2014.11.005

44. Valášek M, Šika Z (2001) Evaluation of dynamic capabilities of machines and robots. Multibody Syst Dyn 6(2):183–202. https://doi.org/10.1023/A:1017520006170

45. Procházka F, Valášek M, Šika Z (2016) Robust sliding mode control of redundantly actuated parallel mechanisms with respect to geometric imperfections. Multibody Syst Dyn 36(3):221–236. https://doi.org/10.1007/s11044-015-9481-8

46. Kautsky J, Nichols NK, van Dooren P (1985) Robust pole assignment in linear state feedback. Int J Control 41(5):1129–1155. https://doi.org/10.1080/0020718508961188